Gold Nanocatalysts

DOI: 10.1002/ange.200906249

Atomically Precise $Au_{25}(SR)_{18}$ Nanoparticles as Catalysts for the Selective Hydrogenation of α,β-Unsaturated Ketones and Aldehydes**

*Yan Zhu, Huifeng Qian, Bethany A. Drake, and Rongchao Jin**

Gold nanoparticles have been found to be capable of catalyzing a variety of reactions, such as selective oxidation and hydrogenation;[1–3] intense efforts have been made in recent years in hope of unravelling the origin of the catalytic properties of gold nanoparticles.[4–7] However, in most studies the nanoparticles are polydispersed; even in the best case the particle dispersity is still about 5%. Therefore, the observed catalytic properties of Au nanoparticles reflect only an ensemble average. Hitherto, there has been no success in preparing atomically monodisperse gold nanoparticle catalysts. The polydispersity of Au nanoparticles and their unknown surface structure preclude the precise correlation of particle structure and electronic properties with their catalytic properties. Thus, in order to understand the origin of their catalytic properties, it is critical to first obtain atomically precise Au nanoparticles.

We have recently succeeded in preparing atomically precise, thiolate-stabilized gold nanoparticles (referred to as $Au_n(SR)_m$, where n and m represent the number of gold atoms and ligands, respectively).[8–11] These ultrasmall nanoparticles constitute a well-defined system and may be utilized for catalysis. On the basis of their crystal structures, these Au particles will permit a correlation of particle structure with catalytic properties and an identification of catalytically active sites on the particle; the latter has long been pursued in nanocatalysis, but active sites are difficult to determine with conventional polydisperse nanoparticles since the particle surface structure is unknown.

Among the series of $Au_n(SR)_m$ nanoparticles, we have solved the crystal structure of Au_{25} nanoparticles stabilized by thiolate ligands ($Au_{25}(SR)_{18}$, where SR denotes thiolate) and also have studied their electronic structure.[12–14] As these particles are well defined and their crystal structure is known, we should be able to study some fundamental aspects of gold nanoparticle catalysis. The Au_{25} structure[12] can be viewed as a Au_{13} icosahedral core (which is electron-rich) encapsulated by an incomplete shell consisting of the exterior 12 gold atoms (which are electron-deficient).[12–14] We speculate that the electron-rich Au_{13} core may facilitate the adsorption and activation of the C=O bond based on literature work,[15,16] and owing to the low coordination, the exterior-shell Au atoms may provide a favorable environment for the adsorption and dissociation of H_2.[17] This implies that Au_{25} particles may be new catalysts for the hydrogenation of the C=O bond in ketones or aldehydes. Our results indeed demonstrate that thiolate-stabilized Au_{25} particles can catalyze the hydrogenation of the C=O bond. More importantly, this work gives insight into the fundamental aspects of gold nanoparticle catalysis since we have already solved the crystal structure of Au_{25}.[12]

Herein, we report on the selective hydrogenation of α,β-unsaturated ketones (e.g. benzalacetone) as a target reaction to investigate the catalytic performance of Au_{25} particles. The resulting unsaturated alcohol products are valuable intermediates for the production of perfumes and flavors. Previously, conventional supported gold nanoparticle catalysts have been demonstrated to be capable of the selective hydrogenation of α,β-unsaturated ketones; predominantly α,β-unsaturated alcohols form, but also side products—saturated ketones from C=C hydrogenation as well as saturated alcohols from further hydrogenation—have been reported.[18–22] Although conventional gold nanoparticles can achieve high conversion and selectivity (>90% for the unsaturated alcohol) in the hydrogenation of α,β-unsaturated ketones, the polydispersity of the Au nanoparticles precludes further studies on the effects of the electronic properties of the nanoparticles on the catalytic performance as well as the nature of the gold atoms at the metal–support interface. Moreover, conventional gold nanoparticles cannot achieve 100% chemoselectivity for the unsaturated alcohol.[22] In our work, we demonstrate that the ultrasmall $Au_{25}(SR)_{18}$ particles (0.97 nm metal-core diameter) can indeed catalyze the hydrogenation of the C=O bond in α,β-unsaturated ketones or aldehydes with 100% chemoselectivity for α,β-unsaturated alcohols. Interestingly, the $Au_{25}(SR)_{18}$ particles are catalytically active for hydrogenation reactions even at low temperatures (e.g. 0°C), which is not possible with conventional Au nanoparticles.

The catalytic reaction was carried out at 0°C (or room temperature) in the solution phase and initiated by introducing H_2 at atmospheric pressure. Both free (unsupported) and oxide-supported $Au_{25}(SR)_{18}$ catalysts were evaluated. The reaction product was analyzed by NMR spectroscopy and GC-MS (Figure 1). NMR analysis identified two components: the unsaturated alcohol product, which shows signals at $\delta =$ 6.55 (β-CH), 6.25 (α-CH), 4.46 (C*H*-OH), and 1.35 ppm (CH_3), and unconverted benzalacetone, which shows peaks at $\delta = 7.51$ ppm (β-CH), 6.70 (α-CH), and 2.32 ppm (CH_3). The integrated peak areas and the coupling constants confirm the

[*] Dr. Y. Zhu, H. Qian, B. A. Drake, Prof. R. Jin
Department of Chemistry, Carnegie Mellon University
4400 Fifth Avenue, Pittsburgh, PA 15213 (USA)
Fax: (+1) 412-268-1061
E-mail: rongchao@andrew.cmu.edu
Homepage: http://www.chem.cmu.edu/groups/jin/

[**] We are grateful for financial support from CMU, AFOSR, and NIOSH.

Supporting information for this article is available on the WWW under http://dx.doi.org/10.1002/anie.200906249.

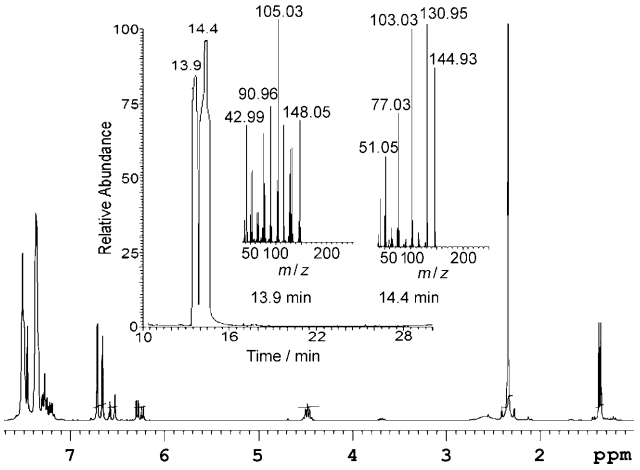

Figure 1. ^{1}H NMR spectrum, GC trace (inset), and mass spectra (smaller insets) of the crude product arising from the hydrogenation of benzalacetone with the Au_{25} catalyst. Two species (unsaturated alcohol and residual starting material) are identified.

assignment. No saturated ketone or saturated alcohol product was detected by NMR spectroscopy. This is also consistent with GC-MS analysis. Only two species were detected by GC, and MS analysis shows that the first eluted species (13.9 min) has a mass signal at *m*/*z* 148 (assigned to the unsaturated alcohol), and that the residual benzalacetone (eluting at 14.4 min) shows a signal at *m*/*z* 145. The conversion and selectivity are quantified on the basis of NMR and GC analysis. For the unsupported $Au_{25}(SC_2H_4Ph)_{18}$ catalyst, the conversion yield (3 h reaction time) is 22% with 100% selectivity for the unsaturated alcohol product (Table 1, entry 1).

Table 1: The catalytic performance of $Au_{25}(SR)_{18}$ catalysts for the selective hydrogenation of benzalacetone with H_2.

Entry	Catalyst	Conv. [%]	Selectivity [%]		
			UA[a]	SK[b]	SA[c]
1	$Au_{25}(SCH_2CH_2Ph)_{18}$	22	100	0	0
2	$Au_{25}(SC_{12}H_{25})_{18}$	20	100	0	0
3	$Au_{25}(SCH_2CH_2Ph)_{18}/Fe_2O_3$	43	100	0	0
4	$Au_{25}(SCH_2CH_2Ph)_{18}/TiO_2$	40	100	0	0
5	$Au_{25}(SCH_2CH_2Ph)_{18}/SiO_2$	19	100	0	0
6	Au nanocrystals[d]	0	–	–	–

Reaction conditions: 1 mg Au_{25} nanoparticle catalyst (or 100 mg oxide powder loaded with 1% wt $Au_{25}(SR)_{18}$ particles), and 0.1 mmol benzalacetone in a mixture of toluene (5 mL) and ethanol (5 mL) stirred at 0°C for 3 h under an atmosphere of H_2. [a] UA: unsaturated alcohol. [b] SK: saturated ketone. [c] SA: saturated alcohol. [d] Nanocrystals are roughly 3 nm in diameter.

Interestingly, thiolate-capped Au nanoparticles roughly 3 nm in diameter (note that these large particles are not atomically monodisperse) are not catalytically active under our experimental conditions (Table 1, entry 6, also see NMR results in Figure S1 in the Supporting Information). These results demonstrate the extraordinary catalytic performance of ultrasmall $Au_{25}(SR)_{18}$ particles, which should be related to their atomic packing structure and electronic properties (see the discussion below). We also investigated the effect of the type of thiolate on the $Au_{25}(SR)_{18}$ particles (e.g. aromatic thiolate vs. long-chain-alkane thiolate); no significant differences were found in terms of the conversion yield and product selectivity (compare entries 1 and 2, Table 1).

The complete selectivity for the unsaturated alcohol product obtained with unsupported $Au_{25}(SR)_{18}$ particles is remarkable. For real-world applications, it would be desirable to use supported catalysts for the ease of recycling and reuse in catalytic reactions. Therefore, we prepared oxide-supported catalysts simply by soaking the oxide powder in a CH_2Cl_2 solution of $Au_{25}(SR)_{18}$ particles, followed by drying (no calcination). The as-obtained $Au_{25}(SR)_{18}$/oxide catalysts were used directly in the reactions. Interestingly, we found that the metal oxide (e.g. Fe_2O_3, TiO_2) supported $Au_{25}(SR)_{18}$ catalysts show significantly higher conversion yields (Table 1, entries 3 and 4) yet the same complete selectivity for the unsaturated alcohol. In contrast, the catalyst on the inert oxide support (SiO_2) showed no enhancement in activity (conversion $\approx$ 19%, entry 5, Table 1). In all cases, no saturated ketone or saturated alcohol was identified by NMR analysis (Figure S1 in the Supporting Information) and GC-MS.

Kinetic studies show that all the three supported catalysts provide maximum conversion at a 3 hour reaction time (Figure S2 in the Supporting Information); the order of the reaction rate, $Au_{25}/Fe_2O_3 > Au_{25}/TiO_2 > Au_{25}/SiO_2$, is consistent with the order of the activity of the catalysts. In both free and supported catalyst systems, longer reaction times were found not to lead to any increase in the conversion (Figure S2 in the Supporting Information), indicating that an equilibrium is reached. Indeed, when an additional benzalacetone was added to the mixture, a similar conversion (about 20% for unsupported catalysts and roughly 40% for supported catalysts) of the newly added reactants was obtained, indicating that the catalysts are not deactivated. We also investigated the recyclability of the catalysts (Figure S2 in the Supporting Information). After six cycles, the supported $Au_{25}(SR)_{18}$ catalysts only show a slight decrease in activity; importantly, the selectivity for unsaturated alcohol remains at 100% throughout the six cycles. Similar results were obtained with unsupported $Au_{25}(SR)_{18}$ catalysts. The robustness of the $Au_{25}(SR)_{18}$ nanoparticle catalysts is of particular importance for their real-world use.

To confirm that the $Au_{25}(SR)_{18}$ nanoparticles do not fragment during the catalytic reaction, we compared the starting catalysts to those after reaction by employing UV/Vis spectroscopy and mass spectrometry. The $Au_{25}(SR)_{18}$ nanoparticles show multiple absorption bands at 670, 450, and 400 nm (Figure 2A), and these bands can serve as spectroscopic fingerprints for comparison purposes; no spectral changes were found after the catalytic reaction. MS analysis (Figure 2B) also confirms that the particles before and after reaction show identical signals at 7394 Da (theoretical mass of $Au_{25}(SC_2H_4Ph)_{18}$: 7394 Da). Taken together, these results confirm that the $Au_{25}(SR)_{18}$ particles remain intact during the reaction; this finding is crucial in understanding the origin of catalysis by $Au_{25}(SR)_{18}$ particles.

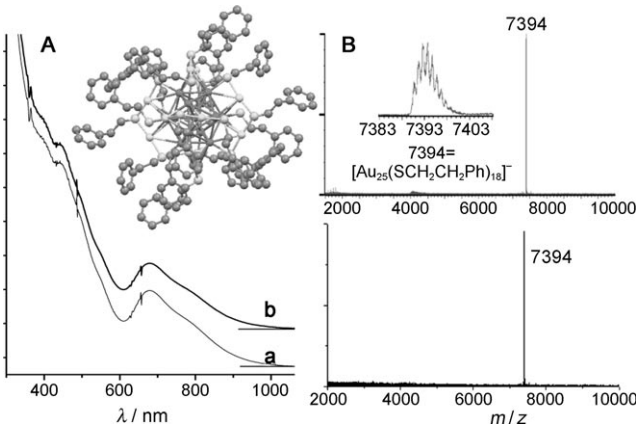

Figure 2. A) UV/Vis spectra of $Au_{25}(SCH_2CH_2Ph)_{18}$ nanoparticles before (a) and after (b) the hydrogenation reaction, and b) after reaction; the inset shows the crystal structure of $Au_{25}(SCH_2CH_2Ph)_{18}$. B) ESI mass spectra of $Au_{25}(SCH_2CH_2Ph)_{18}$ before reaction (upper panel) and after reaction (lower panel), respectively; The inset shows the isotope pattern of $Au_{25}(SCH_2CH_2Ph)_{18}$.

The catalytic properties of intact $Au_{25}(SR)_{18}$ nanoparticles are inspiring and correlate with the particle's atomic packing structure and electronic properties, as we envisioned. On the basis of the crystal structure of $Au_{25}(SR)_{18}$ particles,[12] we propose a mechanism for the $Au_{25}(SR)_{18}$-catalyzed selective hydrogenation of α,β-unsaturated ketones to unsaturated alcohols. The Au_{25} particle possesses a core–shell structure (Figure 2A inset and Scheme 1). Note that there are 20 triangular faces on the Au_{13} icosahedral core. Only 12 facets are face-capped by the exterior 12 Au atoms; thus, eight facets are left open (Scheme 1). These "hole" sites may act as active sites for C=O activation (Scheme 1). A recent theoretical study suggests that the C=O group can coordinate to the surface atoms of Au_{13} clusters, and charge-transfer results in a negatively charged Au_{13} core.[15] Experimental work on the Au_n-catalyzed oxidation of CO with O_2 demonstrates that Au_n particles donate charge to CO and hence, the Au_n core exhibits high catalytic activity.[16] We believe that a similar charge-transfer effect in our system leads to C=O activation.

With respect to the electronic structure of the $Au_{25}(SR)_{18}$ nanoparticles, previous DFT calculations[12–14,23] revealed a discrete, molecule-like electronic structure, which is in striking contrast to the quasi-continuous electronic band structure of Au nanocrystals (e.g. the roughly 3 nm diameter particles used in this work). The multiband UV/Vis spectrum of $Au_{25}(SR)_{18}$ (Figure 2A) is indeed a manifestation of the discrete electronic structure of the particles. DFT calculations assigned the 670 nm absorption band to the HOMO–LUMO transition; note that the HOMO is nearly triply degenerate (excluding spin degeneracy). DFT calculations[14,23] also show a major difference in charge distribution on the Au_{13} core and the Au_{12} shell: the superatomic Au_{13} core possess 8 valence electrons ($1s^21p^6$) and is electron rich, while the exterior Au_{12} shell is electron deficient as a result of electron transfer to sulfur of the thiolate ligand. In contrast to molecule-like $Au_{25}(SR)_{18}$ nanoparticles, the roughly 3 nm Au particles used in our study are crystalline with *fcc* packing and show a surface plasmon absorption band at 520 nm, indicating that the 3 nm gold core is already metallic, as opposed to the semiconducting Au_{25} particles. We propose that the discrete electronic structure of $Au_{25}(SR)_{18}$ and its incomplete Au_{12} exterior shell are responsible for the extraordinary selectivity and activity observed. The eight uncapped Au_3 faces of the icosahedron should favor adsorption of the C=O group by interaction with the O atom of the C=O group in the α,β-unsaturated ketone; electron transfer between Au_{13} and the O atom would activate the C=O bond. Subsequently, the weakly nucleophilic hydrogen attacks the activated C=O group, leading to the unsaturated alcohol product. Overall, the presence of the electron-rich gold core (Au_{13}) favors the selective hydrogenation of the C=O bond over the C=C bond in α,β-unsaturated ketone.

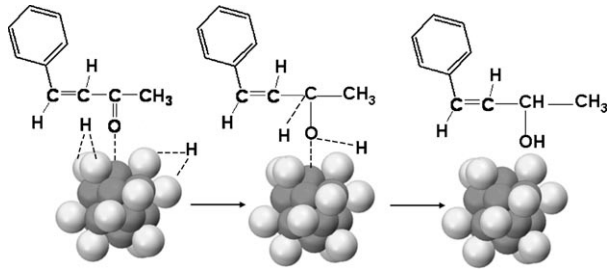

Scheme 1. The proposed mechanism of the chemoselective hydrogenation of α,β-unsaturated ketone to unsaturated alcohol catalyzed by $Au_{25}(SR)_{18}$ nanoparticles. For clarity, the thiolate ligands are not shown. Dark grey: Au atoms of the core; light gray: Au atoms of the shell.

As for H_2 activation, it is thought that the hydrogenation activity of gold catalysts is determined by the step of H_2 dissociation.[24] Theoretical studies have suggested that gold atoms in corner or edge positions can readily activate molecular hydrogen.[25,26] The necessary condition for H_2 dissociation is the existence of low-coordinate Au atoms. Corma et al.[17] presented evidence that H_2 adsorbs and dissociates with small activation barriers on low-coordinate Au atoms situated in the corner positions of Au nanoparticles. Their study supports the idea that a single low-coordinate Au atom can simultaneously interact with the two hydrogen atoms of H_2, and after dissociation, the two H atoms are in bridge positions sharing the low-coordinate gold atom. In the case of Au_{25} particles, the surface Au atoms' low-coordination character (coordination number $N = 3$, c.f. $N = 12$ in bulk gold) should provide a favorable environment for the adsorption and dissociation of H_2, and H_2 dissociation should occur on the Au atoms of the exterior shell (Scheme 1). The two H atoms form two nearly symmetrical Au-H-Au bridges (Scheme 1) based on the study by Corma et al.[17] It is important to note that during the activation/reaction process catalyzed by $Au_{25}(SR)_{18}$, H_2 dissociation does not induce any significant deformation of the $Au_{25}(SR)_{18}$ catalyst surface (Figure 2); in other words, the $Au_{25}(SR)_{18}$ particle retains its integrity (otherwise one would observe changes in the UV/Vis spectrum).

To further support our attribution of the catalytic properties of $Au_{25}(SR)_{18}$ nanoparticles to the unique geometrical and

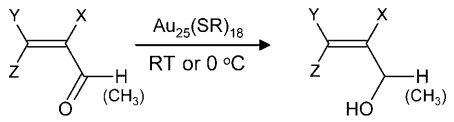

Scheme 2. $Au_{25}(SR)_{18}$-catalyzed hydrogenation of a range of substituted α,β-unsaturated ketones and aldehydes. X = H or CH_3, Y = H, CH_3, or Ph, and Z = H or CH_3.

electronic structures of these particles, we have further investigated a number of representative substituted α,β-unsaturated ketones and aldehydes (Scheme 2, Table S1 in the Supporting Information). Complete (100%) selectivity was observed in all cases except crotonadehyde (91% selectivity for the allylic alcohol). For future work, we plan to perform full density functional theory (DFT) calculations incorporating α,β-unsaturated ketone (aldehyde) and H_2 to find out more details on the C=O and H_2 activation and reaction mechanism.

In summary, we have demonstrated the catalytic capability of thiolate-stabilized, well-defined $Au_{25}(SR)_{18}$ nanoparticles for the chemoselective hydrogenation of α,β-unsaturated ketones and aldehydes to unsaturated alcohols with complete (100%) selectivity (except crotonadehyde, 91% selectivity for allylic alcohol). The core–shell structure of the $Au_{25}(SR)_{18}$ particles (i.e. Au_{13} core/Au_{12} shell) and their unique electronic properties (i.e. electron-rich Au_{13} core and low-coordinate (N = 3) surface gold atoms) are thought to be responsible for the observed catalytic performance of $Au_{25}(SR)_{18}$ nanoparticles. Future calculations and experimental work are expected to offer important insights into the fundamental mechanism of gold nanoparticle catalysis. The atomically precise, ultrasmall $Au_n(SR)_m$ particles hold promise in their utility as a new type of gold nanocatalysts that offer high selectivity for certain reaction processes. An atomic-level understanding on how the crystal structure of the $Au_n(SR)_m$ nanoparticles, the bonding effect of surface atoms, and the electronic properties affect the catalytic properties of gold nanoparticles will eventually aid in the design of nanocatalysts for specific reactions.

Experimental Section

$Au_{25}(SR)_{18}$ catalysts: $Au_{25}(SR)_{18}$ nanoparticles were synthesized following a kinetically controlled approach.[8] UV/Vis absorption spectra (190–1100 nm) were recorded using a Hewlett-Packard (HP) 8453 diode-array spectrophotometer. Electrospray ionization mass spectra were acquired using a Waters Q-TOF mass spectrometer equipped with Z-spray source. The as-prepared nanoparticles were used as homogeneous catalysts, and the supported catalysts were prepared as follows: 100 mg of the oxide support (in powder form) was impregnated by soaking in a solution of 1 mg $Au_{25}(SR)_{18}$ nanoparticles in CH_2Cl_2 (ca. 10 mL) in a sealed vial for one day, followed by drying; no calcination was done.

Catalyst testing: In a 50 mL three-neck glass flask benzalacetone (0.1 mmol) was dissolved in a mixed solvent (5 mL toluene and 5 mL ethanol). The gold catalyst, either 1 mg $Au_{25}(SR)_{18}$ (unsupported), or 100 mg catalyst on an oxide support (1% wt loading of $Au_{25}(SR)_{18}$) was added. The reaction was initiated by introducing a H_2 flow (under atmospheric pressure). Reaction temperature: 0°C or room temperature (no difference in catalytic activity or selectivity was found). The reaction was typically allowed to proceed under continuous H_2 flow for roughly 3 h (unless otherwise noted). The crude products were analyzed by ^{1}H NMR spectroscopy and GC-MS. NMR spectroscopy was conducted on a Bruker Avance 300 MHz instrument. GC mass spectra were obtained using a Thermo Finnigan Trace GC 2000 and an Rxi-XLB chromatographic column.

Received: November 6, 2009
Published online: January 14, 2010

Keywords: gold · heterogeneous catalysis · hydrogenation · nanoparticles · structure–activity relationships

[1] M. Haruta, *Nature* **2005**, *437*, 1098 – 1099.
[2] A. Corma, P. Serna, *Science* **2006**, *313*, 332 – 334.
[3] A. S. K. Hashmi, G. J. Hutchings, *Angew. Chem.* **2006**, *118*, 8064 – 8105; *Angew. Chem. Int. Ed.* **2006**, *45*, 7896 – 7936.
[4] G. C. Bond, C. Louis, D. T. Thompson in *Catalysis by Gold*, *Vol. 6* (Ed: G. J. Hutchings), Imperial College, London, **2006**, pp. 161 – 336.
[5] *Nanocatalysis* (Eds.: U. Heiz, U. Landman), Springs, New York, **2007**.
[6] W. Xu, J. S. Kong, Y. E. Yeh, P. Chen, *Nat. Mater.* **2008**, *7*, 992 – 996.
[7] J. C. Fierro-Gonzalez, B. C. Gates, *Chem. Soc. Rev.* **2008**, *37*, 2127 – 2134.
[8] a) M. Zhu, E. Lanni, N. Garg, M. E. Bier, R. Jin, *J. Am. Chem. Soc.* **2008**, *130*, 1138 – 1139; b) Z. Wu, J. Suhan, R. Jin, *J. Mater. Chem.* **2009**, *19*, 622 – 626.
[9] a) H. Qian, M. Zhu, U. N. Andersen, R. Jin, *J. Phys. Chem. A* **2009**, *113*, 4281 – 4284; b) H. Qian, Y. Zhu, R. Jin, *ACS Nano* **2009**, *3*, 3795 – 3803.
[10] M. Zhu, H. Qian, R. Jin, *J. Am. Chem. Soc.* **2009**, *131*, 7220 – 7221.
[11] H. Qian, R. Jin, *Nano Lett.* **2009**, *9*, 4083 – 4087.
[12] M. Zhu, C. M. Aikens, F. J. Hollander, G. C. Schatz, R. Jin, *J. Am. Chem. Soc.* **2003**, *130*, 5883 – 5885.
[13] C. M. Aikens, *J. Phys. Chem. C* **2008**, *112*, 19797 – 19800.
[14] M. Zhu, C. M. Aikens, M. P. Hendrich, R. Gupta, H. Qian, G. C. Schatz, R. Jin, *J. Am. Chem. Soc.* **2009**, *131*, 2490 – 2492.
[15] M. Okumura, Y. Kitagawa, K. Yamaguchi, M. Haruta, *Chem. Phys. Lett.* **2008**, *459*, 133 – 136.
[16] H. Tsunoyama, N. Ichikuni, H. Sakurai, T. Tsukuda, *J. Am. Chem. Soc.* **2009**, *131*, 7086 – 7093.
[17] A. Corma, M. Boronat, S. Gonzalez, F. Illas, *Chem. Commun.* **2007**, 3371 – 3373.
[18] G. J. Hutching, J. E. Bailie, *Chem. Commun.* **1999**, 2151 – 2152.
[19] C. Mohr, H. Hofmeister, J. Radnik, P. Claus, *J. Am. Chem. Soc.* **2003**, *125*, 1905 – 1911.
[20] C. Milone, R. Ingoglia, L. Schipilliti, C. Crisafulli, G. Neri, S. Galvagno, *J. Catal.* **2005**, *236*, 80 – 90.
[21] C. Sui-seng, A. Hadzovic, A. J. Lough, R. H. Morris, *Dalton Trans.* **2007**, 2536 – 2541.
[22] P. G. N. Mertens, P. Vandezande, X. Ye, H. Poelman, I. F. J. Vankelecon, D. E. DeVos, *Appl. Catal. A* **2009**, *355*, 176 – 183.
[23] J. Akola, M. Walter, R. L. Whetten, H. Hakkinen, H. Gronbeck, *J. Am. Chem. Soc.* **2008**, *130*, 3756 – 3757.
[24] R. Zanella, C. Louis, S. Giorgio, R. Touroude, *J. Catal.* **2004**, *223*, 328 – 339.
[25] C. Mohr, H. Hofmeister, J. Radnik, P. Claus, *J. Am. Chem. Soc.* **2003**, *125*, 1905 – 1911.
[26] L. Andrews, *Chem. Soc. Rev.* **2004**, *33*, 123 – 132.

